Plasma-Induced Quantum Well Intermixing for Monolithic Photonic Integration

Hery Susanto Djie, *Member, IEEE,* and Ting Mei, *Member, IEEE*

***Abstract*—Plasma-induced quantum well intermixing (QWI) has been developed for tuning the bandgap of III–V compound semiconductor materials using an inductively coupled plasma system at the postgrowth level. In this paper, we present the capability of the technique for a high-density photonic integration process, which offers three aspects of investigation: 1) universality to a wide range of III–V compound material systems covering the wavelength range from 700 to 1600 nm; 2) spatial resolution of the process; and 3) single-step multiple bandgap creation. To verify the monolithic integration capability, a simple photonic integrated chip has been fabricated using Ar plasma-induced QWI in the form of a two-section extended cavity laser diode, where an active laser is integrated with an intermixed low-loss waveguide.**

***Index Terms*—Inductively coupled plasma (ICP), photonic integrated circuits (PICs), quantum well, quantum well intermixing (QWI).**

I. Introduction

THE ABILITY TO modify the bandgap energy across the single substrate is a key requirement for monolithic integration of multiple photonic devices. The quantum well intermixing (QWI) technique has generated considerable interest due to its simplicity and effectiveness to tune the quantum well (QW) properties at the postgrowth level for optoelectronic and photonic integrated circuit (PIC) applications [1]. A strong motivation to develop an effective QWI exists, since QWI is a simple and reliable process at the postgrowth level to tune QW properties. The emerged technology of QWI in the past decades, such as impurity-induced disordering (IID) [2], [3], impurity-free vacancy disordering (IFVD) [4], sputtered silica-induced intermixing [5], and pulsed-photoabsorption-induced disordering (PPAID) [6] have been utilized in wide application for PICs, such as the widely tunable sampled-grating distributed Bragg reflector laser device [7].

The development of high-density plasma, such as the inductively coupled plasma (ICP) machine, enables the use of low ion bombardment energy with high ion bombardment fluxes. ICP reactors produce high-density plasmas $(10^{10} - 10^{12}\ \mathrm{cm}^{-3})$ at low gas pressure (<tens of millitorrs). ICPs have been used for high-etch-rate, low-etch-damage applications in a wide variety of semiconductor materials including dielectrics and III–V semiconductors and for depositing various dielectric materials. The use of plasma-enhanced QWI is attractive, since the low-energy (with hundreds of electronvolts of ion impact energy) ions generated in the plasma chamber produces no direct damage to the QW active region, thereby promising high-quality photonic devices for PIC application. Recently, a QWI technique using a inductively coupled argon (Ar) plasma process has been successfully developed, and it has proven to be very effective to tune the bandgap energy of InP-based QW materials [8]–[10]. Initial work has been done using H_2 plasma glow discharge in a reactive ion-etching (RIE) system on GaAs/AlGaAs structures. Up to eight cycles of H_2 plasma exposure and annealing is required to produce a maximum bandgap wavelength blue-shift of about 24 nm [11]. Ar gas is used, since it is a noble gas with a relatively high atomic weight to produce a high surface defect density for a high degree of intermixing. When Ar ions are introduced to the semiconductor material, they create point defects, including vacancies, interstitials, and vacancy-interstitial (Frenkel) pairs. This technique utilizes the generation of mobile point defects far from the active QWs region, as the Ar ions may knock ions off its crystal site of sample to produce either single isolated vacancy or group of vacancies. During the subsequent annealing, the interstitials can effectively propagate from one lattice to another lattice site in the random walk motion through the kick-out mechanism [12]. The substitutional–interstitial diffusion down to the active QWs region subsequently will promote intermixing between the QWs and their barriers to form alloy semiconductors. This intermixing process results in an increase in the QW energy bandgap. In addition to the annealing process, the annealing treatment also recovers crystal damage on the sample surface induced by the QWI technique and the intermixed device does not suffer significant optical degradation.

In this paper, we report the attractive characteristics of QWI effect of inductively coupled Ar plasma on various QW structures for the monolithic integration of multiple photonic devices. In order to have a better understanding of the high-density effect to QWI, the plasma process mechanism, the QWI universality, the spatial resolution improvement, and the control of intermixing degree, we further characterize the plasma-induced QWI process using low-temperature photoluminescence (PL), a room temperature (RT) PL map, and micro-Raman spectroscopy (MRS). To verify the integration capability, we fabricated the extended cavity lasers, where the passive waveguide is formed by selective intermixing process.

II. Experiments

Samples of an InGaAs/InGaAsP QWs laser structure on InP substrate with the emission wavelength around 1.55 μm are used in this study. Other material systems of InGaAs/InAlGaAs QWs laser structure on InP substrate and GaAs/AlGaAs structure QWs laser structure on GaAs substrate are adopted to further

Manuscript received July 16, 2004; revised January 18, 2005.

H. S. Djie is with the School of Electrical and Electronic Engineering, Nanyang Technological University, Singapore 639798 (e-mail: hery@pmail.ntu.edu.sg).

T. Mei is with the School of Electrical and Electronic Engineering, Nanyang Technological University, Singapore 639798 (e-mail: etmei@ntu.edu.sg).

Digital Object Identifier 10.1109/JSTQE.2005.845611

investigate the QWI mechanism using high-density plasma and its effect and the universality of plasma-induced QWI process. The lattice-matched InGaAs/InGaAsP QWs laser structure was grown by metal–organic vapor phase epitaxy (MOVPE) on (100) oriented n^+-type S-doped InP substrate. The QW active region consists of five periods of 5.5-nm-wide $In_{0.53}Ga_{0.47}As$ QWs with 12-nm-thick $In_{0.77}Ga_{0.23}As_{0.49}P_{0.51}$ barriers. The active region is sandwiched by step-graded index waveguide core consisting of InGaAsP confining layers. The thicknesses of these confining layers (from the QWs outward) are 50 and 80 nm, respectively. The structure was completed by an upper cladding InP layer of 1.37-μm-thick doped with Zn to $7.3 \cdot 10^{17}$ cm^{-3}. The contact layer consists of 50-nm-thick InGaAsP (Zn doped to $2 \cdot 10^{18}$ cm^{-3}) and 100-nm-thick InGaAs (Zn doped to $1.8 \cdot 10^{19}$ cm^{-3}). The samples resulted in a PL peak at 1.43 ± 0.02 μm at 77 K.

The lattice matched InGaAs/InAlGaAs QWs laser structure was grown by molecular beam epitaxy (MBE) on a Si-doped InP substrate. The thicknesses of InP buffer layer (Si doped to $1 \cdot 10^{18}$ cm^{-3}) and lower cladding layer (Si doped to $3 \cdot 10^{18}$ cm^{-3}) were 500 and 300 nm, respectively. The QW active region consists of six 7-nm-wide $In_{0.53}Ga_{0.47}As$ wells separated by 8-nm-thick $In_{0.53}Al_{0.27}Ga_{0.2}As$ barriers. The active region was sandwiched by 100-nm-thick $In_{0.53}Al_{0.27}Ga_{0.2}As$ waveguide cores (Zn doped to $2 \cdot 10^{17}$ cm^{-3}). It was completed by a 100-nm-thick InP upper cladding layer (Zn doped to $7 \cdot 10^{17}$ cm^{-3}) followed by a 50-nm-thick InGaAsP etch stop layer (Zn doped to $1 \cdot 10^{18}$ cm^{-3}) and a 1200-nm-thick InP upper cladding layer (Zn doped to $1 \cdot 10^{18}$ cm^{-3}). The contact layer consists of 50-nm-thick InGaAsP (Zn doped of $2 \cdot 10^{18}$ cm^{-3}) and 200-nm-thick InGaAs (Zn doped to $1.4 \cdot 10^{19}$ cm^{-3}). The QW area was undoped thus forming a P-I-N structure with the intrinsic region restricted to the QW layers. The samples resulted in a PL peak at 1.55 ± 0.002 μm at RT and 1.43 ± 0.002 μm at 77 K, respectively.

A GaAs/AlGaAs QWs laser structure, grown by MOVPE, is used to study the plasma-induced QWI in the short wavelength region of 0.86 μm. The active region was undoped and consisted of 25 periods of 10 nm-wide GaAs QWs with 10-nm-thick $Al_{0.2}Ga_{0.8}As$ barriers. The top and bottom $Al_{0.2}Ga_{0.8}As$ layers were 100 nm thick to complete the waveguide core. Both upper and lower cladding $Al_{0.4}Ga_{0.6}As$ layers were 1500 nm thick and doped to a concentration of $8 \cdot 10^{17}$ cm^{-3} and $9 \cdot 10^{17}$ cm^{-3} using carbon and silicon, respectively. The top contact layer is a layer of 100-nm-thick GaAs doped with Zn to $1.3 \cdot 10^{19}$ cm^{-3}. This as-grown material exhibited a 77 K PL peak at about 810 ± 2 nm.

The GaAs/AlGaAs multiwidth QWs damage probe structure is adopted to study the plasma-induced damage mechanism and intermixing process by tracing the damage distribution range [13], [14]. The QW structure was grown on a semi-insulating GaAs substrate by MBE, consisting of five undoped QWs labeled as QW1, QW2, QW3, QW4, and QW5 by sequence from the top to the substrate, with well widths of 9.5, 7, 4, 3 and 2.5 nm, respectively. The $Al_{0.3}Ga_{0.7}As$ barriers are 300 nm thick, except the one between QW4 and QW5, which is 1000 nm thick. With this configuration, the QWs are located accordingly in order to asses the damage distribution range due to QWI process, with QW5 as a reference PL signal. The structure was completed by a layer of 100-nm GaAs cap layer on the top.

The ICP system used in this experiment uses inductive coil to generate high-density "remote" plasma with no direct contact between the plasma and the substrate. The 13.56-MHz RF and ICP power supply can provide the independent control on ion bombardment energy and ion current density with power up to 500 and 3000 W, respectively. The ICP parameter settings for the experiments were 100 sccm Ar flow rate, 80 mtorr chamber pressure, 480 W RF power, 730 V RF-induced dc bias and 500 W ICP power. After Ar plasma exposure, the samples were annealed using a single-step annealing in a flowing nitrogen ambient. Two fresh pieces of GaAs proximity caps were used to provide an As overpressure environment during the annealing process and further to prevent the sample surface from outdiffusion. The annealing conditions were determined from a thermal stability test performed on as-grown samples. A control sample refers to the annealed sample without plasma exposure to determine a bandgap shift due to the annealing effect.

The experiment results are analyzed using the low-temperature and RT PL spectroscopy. The single-point PL measurements are carried out at 4 K and 77 K using a 50-μm-diameter optical fiber as a signal probe, an Nd : YAG laser (1.064 μm) for excitation, a monochromator, and a TE-cooled InGaAs photodetector associated with a lock-in amplifier. The PL map at RT enables the observation of the spatial bandgap profile after selective QWI process and its uniformity. The PL system scan has a resolution of 100 μm due to the limitation of stage controller. The illumination wavelength is at 1.064 μm using a Q switch laser with a $\sim$ 10–μm spot diameter of the focused laser beam and 6.6 mW output power. MRS is carried out at RT to study the spatial resolution of selectively intermixed material using Renishaw model inVia Reflex. The MRS line mapping across the intermixing boundary was taken in the backscattering configuration using the laser physics Ar laser of 514.5 nm as the excitation source with a 100$\times$ objective (Leica 100$\times$ Nplan), giving a spot size diameter of $\sim$ 0.4 μm.

III. Universal High-Density Plasma Enhanced QWI

In order to study the effect of high-density plasma application of the ICP system, the InGaAs/InGaAsP and the GaAs/AlGaAs QWs laser structures were exposed in an ICP chamber without ICP power (pure RF power and thus low plasma density) and with ICP power (thus high-density plasma). All other affecting parameters of ICP reactor were kept constant except the ICP power, enabling a comparative study on the effect of ICP application to the intermixing results. Without ICP power application, a larger bandgap shift can be achieved only by increasing the energy of bombarding ions, while with ICP power application, the ion density acts as a factor for bandgap shift control [8]. The ICP application at the constant RF power decreases the RF bias while increasing the ion dose and plasma radiation, which are estimated to be several orders larger than the traditional ion-implantation method [15].

Fig. 1(a) shows the PL spectra comparison from the InGaAs/InGaAsP laser QWs structure at 4 K after intermixing at ICP power of 0 and 250 W. The RF-induced dc bias operation was -840 V at pure RF power and was reduced to -780 V

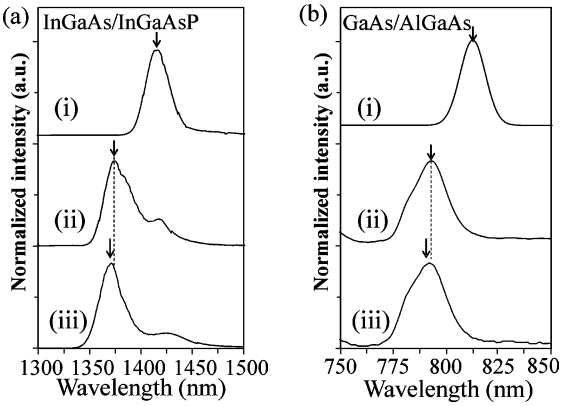

Fig. 1. Low-temperature PL spectra measured from (i) the as-grown material, and the materials after intermixing (ii) without ICP application and (iii) with ICP application in plasma exposure for the materials of (a) InGaAs/InGaAsP QWs and (b) AlGaAs/GaAs QWs.

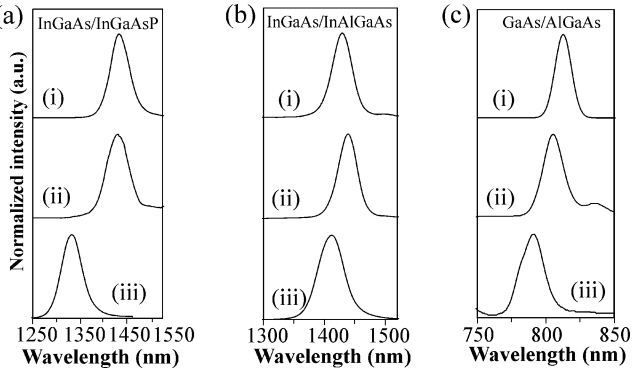

Fig. 2. Normalized PL spectra at 77 K for (i) as-grown; (ii) annealed only; and (iii) intermixed materials from various laser structures: (a) InGaAs/InGaAsP QWs. (b) InGaAs/InAlGaAs QWs. (c) GaAs/AlGaAs QWs.

when the ICP power was 250 W. The two intermixed PL spectra produce a comparable bandgap shift of 60 and 62 nm as compared to the as-grown spectrum for exposed material without and with ICP power application, respectively. The similar behavior can be observed from Fig. 1(b) for the case of GaAs/AlGaAs QWs laser structure that increasing the ICP power from 0 to 500 W produces the bandgap shift blue-shift of 18 and 20 nm for samples being exposed to plasma without and with ICP power application, respectively. The samples only exhibit a small increase in bandgap energy after annealing without plasma exposure as compared to the as-grown material. The annealing induced bandgap shifts on the samples are attributed to the in-diffusion of point defects from the substrate, grown-in defects on the epilayers, and the impurity. The comparable bandgap blue shifts for both InGaAs/InGaAsP and GaAs/AlGaAs have been achieved using the ICP power application instead of pure RF power. The RF-induced dc bias reduction leads to less effect of bombarding ion energy to the induced damage, and thus this suggests that the high plasma density due to ICP application contributes to promote QWI on both QW structures. The application of ICP power induces more damage due to the plasma radiation together with high ion current density on the samples such as the relevant observation reported elsewhere using high-density plasma process in an electron cyclotron resonance (ECR) system [16]. The linewidth profile of PL spectra of the intermixed samples with ICP power application are slightly less than those without the ICP power application on both InGaAs/InGaAsP and GaAs/AlGaAs structures, suggesting a good optical quality preservation using the Ar plasma exposure at a high-density plasma.

The universality of plasma-induced QWI has also been investigated using other III–V material systems. Previous studies observed that the magnitude of the created defects increases with the plasma exposure time in the III–V material system [13], [14]. Earlier experimental data in InGaAs/InP QWs shows that the bandgap shift due to Ar plasma exposure from PL spectra saturates as the exposure time increases [15], indicating the saturation of created defect has been reached at this level [17]. The bandgap shift saturation occurs after 1 min in InGaAs/InAlGaAs and GaAs/AlGaAs structures and 5 min in InGaAs/InGaAsP structures for plasma condition of 500 W ICP power and 480 W RF power. This points out the universal creation of beneficial defects to the III–V materials occurred in the different time scale.

Fig. 2 depicts the PL spectra of the as-grown, the control (annealed only), and the intermixed (exposed and annealed) samples for laser structures of InGaAs/InGaAsP QWs, InGaAs/InAlGaAs QWs, and GaAs/AlGaAs QWs. Correspondingly, the plasma exposure durations are 5, 2, and 1.5 min and the annealing conditions are 600 °C for 2 min, 650 °C for 2 min, and 860 °C for 0.5 min. The annealing condition for each structure was chosen below a critical temperature from the thermal stability test, beyond which the as-grown sample started to experience appreciable bandgap shift due to other effects. After the exposure and subsequent annealing, the samples exhibit bandgap blue-shifts with inappreciable linewidth broadening, indicating the enhancement of intermixing rate due to the plasma-induced damage on the QW systems, in the form of mobile point defects, rather than the thermal induced interdiffusion. The obtained optimum bandgap shifts are 100 nm (65 meV), 66 nm (42 meV), and 23 nm (43 meV) for the three materials. The difference in the bandgap shift could be attributed to the different band offset of the three material structures. In addition to that, the defect diffusion in InGaAs/InGaAsP material is more efficient to promote intermixing in agreement with the study of defect diffusion using InP- and AlGaAs-based ion implantation induced QWI process [18]. The bandgap shift in the GaAs/AlGaAs system is comparable to the result achieved in the GaAs/AlGaAs system using multicycle H_2 plasma exposure and annealing [11]. These results demonstrate the effectiveness and the universality of inductively coupled Ar plasma-induced QWI to alter the bandgap energy of III–V materials.

At low ion energy (hundreds of electronvolts), the majority of the impinging ions of Ar plasma is stopped within the first few atomic monolayers of material and may cause lattice disruption and damage up to a depth of a few tens of nanometers [19], thus avoiding direct damage to the QW active regions which are located deeper than 1.5 μm below the sample surface. We further investigate the plasma-induced damage mechanism causing the intermixing using GaAs/AlGaAs multiwidth QWs damage probe structure. Fig. 3 shows the comparison of 77 K PL spectra

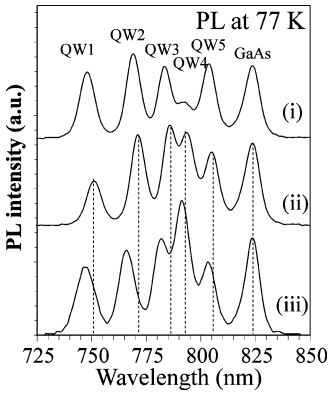

Fig. 3. 77 K normalized PL spectra obtained from multiwidth GaAs/AlGaAs QWs probe structures. (i) As-grown material. (ii) After high-density plasma exposure for 1 min. (iii) Subsequent annealing to the exposed sample at 765 °C for 2 min. The PL spectra are normalized to the deepest QW (QW5), which acts as a reference signal.

normalized to the PL peak intensity of the deep most QW (QW5) after exposure at 500 W ICP power for 1 min and subsequent annealing. The annealing condition at 765 °C for 2 min has no pronounced thermal shift of QWs. Fig. 3(i) clearly exhibits six peaks for the as-grown QWs probe structure, one for each QW and the GaAs substrate at 822 nm. After exposure [Fig. 3(ii)], the PL intensity of the shallowest QW (QW1) is clearly reduced by 32%, suggesting that the high-density plasma generates the near surface damage at a depth of more than 0.4 μm, in the form of mobile point defects, leading to an increase in nonradiative recombination and a decrease in PL intensity. Upon annealing [Fig. 3(iii)], the PL intensity of QW1 is recovered to the level close to that of the as-grown sample with the shift of the PL peak for all the QWs. The PL intensity recovery indicates that the annealing process has restored the created surface damage during plasma exposure. Upon annealing, the PL peaks of all QWs have been blue-shifted. The result suggests that the created damage, in the form of mobile point defects, propagates deeper to the deep-most QW (QW5) more than 2.32 μm and promote the intermixing between wells and barriers.

IV. Spatial Resolution Study

Recently, there has been increasing interest in scaling the PICs monolithically on a single wafer. In order to achieve high-density photonic integration, the QWI process must be capable of tuning the material bandgap with high spatial selectivity. For example, the spatial resolution requirement of quasi-phase-matching grating for the second harmonic generation would be in the micrometer range [20], [21]. However, the selective intermixing induced by the interdiffusion of the near surface defects tends to give a low spatial resolution due to the spreading of mobile point defects formed on the top surface in the lateral direction as they propagate to the QW region during annealing. Thus, interruption of QW epitaxy growth process and a sacrificial layer removal are required to improve a high spatial resolution QWI [3]. Therefore, the investigation on the spatial resolution of plasma-induced QWI and its improvement is necessary to be carried out.

Two samples of InGaAs/InGaAsP QWs laser structures with dimensions of 8×8 mm^2 were coated by a 300-nm-thick

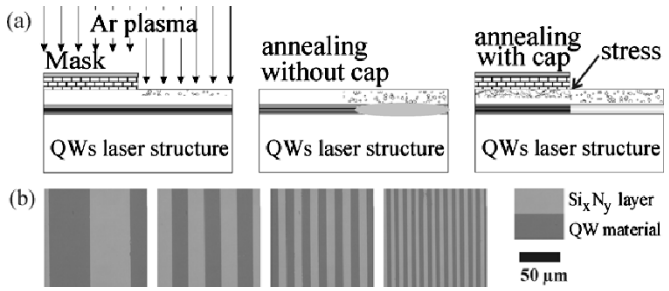

Fig. 4. (a) Si_xN_y patterns with variable stripe widths defined on the InGaAs/InGaAsP QWs laser structure after lithography and subsequent dry etch process using RIE machine, containing stripe widths of 50, 20, 10, and 5 μm. (b) The schematic representation of the creation of high-density surface defects and subsequent annealing process with and without the presence of the stress-inducing dielectric mask.

Si_xN_y layer using a plasma-enhanced chemical vapor deposition (PECVD) as an intermixing mask. The Si_xN_y material was chosen due to its minimal solubility of group III atoms, thus minimizing the III–V species outdiffusion from the area patterned with the dielectric mask [22]. After the lithography process, an RIE process using CF_4/O_2 mixture followed by the diluted HF solution was done to produce 2×2 mm^2 arrays of Si_xN_y patterns with different stripe widths of 50, 20, 10 and 5 μm, as depicted in Fig. 4(a). By varying the width of the patterned stripes, the sum of intermixed and unintermixed PL spectra can be collected as a direct evidence of spatial resolution. The samples were exposed for 5 min under Ar plasma using 500 W ICP power.

Prior to annealing, the Si_xN_y pattern was removed in one sample using diluted HF solution, while it was preserved in another sample. During high-temperature annealing, the stress field on the film/QW material interface is modified due to the mismatch of the linear thermal expansion coefficient between Si_xN_y layer ($\sim 2.8 \cdot 10^{-6}\,^{\circ}\mathrm{C}^{-1}$) and InP-based material ($\sim 4.6 \cdot 10^{-6}\,^{\circ}\mathrm{C}^{-1}$). A study by Pepin *et al.* reveals that the Si_xN_y layer deposited on GaAs material during the high annealing temperature is at a very high tensile stress ($\sim$3.5 GPas) as estimated from the measured Si_xN_y intrinsic stress, σ_{in}, at RT after deposition [23]. We believe that the Si_xN_y layer deposited onto the QW material is similar to the case of GaAs material that Si_xN_y is under compressive strain during annealing, while the QW material under the trench is under tensile strain. This generates the modulation of the stress field distribution under Si_xN_y masked region oriented in a direction perpendicular to the sample surface. The amplitude of stress is modulated strongly between the masked and unmasked region and enhanced compressive stress exists at the Si_xN_y pattern edges, as shown in the previous calculation of strain distribution using the finite-element method [24].

As illustrated in Fig. 4(b), a 300-nm-thick Si_xN_y mask patterned on the sample surface is expected to block the point defect creation during the plasma exposure in the masked region and minimizes the defect diffusion in the lateral direction due to the stress effect during the annealing process. The Si_xN_y mask here can be utilized as a stress-inducing dielectric mask during annealing. The created surface defects propagate downward to the QW active region to promote intermixing during annealing, and in the meantime the lateral diffusion of defects smear the boundary of intermixing area so that the two PL peaks tend to merge as the pattern pitch are getting smaller. Therefore, by

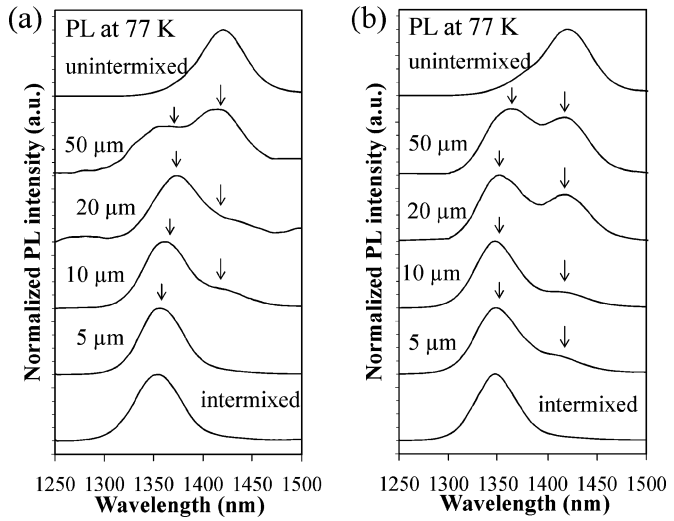

Fig. 5. PL spectra of intermixed InGaAs/InGaAsP QWs materials by varying the stripe widths of dielectric masks. (a) Annealed without a dielectric mask. (b) Annealed with a dielectric mask. The 50-μm-diameter multimode optical fiber was used as a PL probe at the temperature measurement of 77 K.

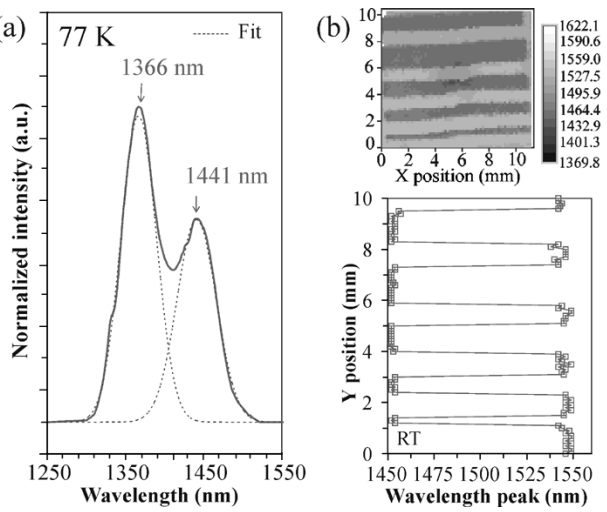

Fig. 6. PL spectrum at 77 K (solid line) of InGaAs/InGaAsP QWs taken from the intermixing boundary using 50-μm-diameter optical fiber as a PL probe and its Gaussian fitted curves (dotted line). (b) RT two-dimensional PL maps (above) and the one-dimensional line map (below) of peak wavelength emission taken across selectively intermixed material with a system resolution of 100 μm.

varying the stripe width and observing the disappearance of the intermixed PL peaks, the spatial resolution of the process can be determined [25].

PL spectra at 77 K were then measured from each array using a 50-μm-diameter multimode optical fiber as a probe. Due to the fiber spot size dimension, the PL spectra from the patterned samples contain PL signals from both masked (unintermixed) and unmasked (exposed, thus intermixed) regions. Fig. 5 shows the comparison of PL spectra from arrays annealed with and without the presence of a stress-inducing dielectric mask with different stripe widths. The unintermixed and intermixed PL spectra refer to the PL signal probed from relatively large areas of masked and unmasked portions of the same substrate, respectively, are included for comparison. The PL spectra of the patterned area exhibit two peaks corresponding to both intermixed and unintermixed regions. The differential bandgap shifts between intermixed and unintermixed regions are 74 and 66 nm for annealed samples with and without stress-inducing dielectric mask, respectively. The sample with stress-inducing dielectric mask exhibited a larger bandgap shift due to the interdiffusion enhancement caused by the group V out diffusion from the presence of a small gap between sample and GaAs proximity cap during annealing. The appearance of well-resolved dual peaks suggested that high selectivity is obtainable in QW samples using a stress-inducing dielectric mask. For the sample annealed without a stress-inducing dielectric mask, the separation of two peaks clearly observed for the stripe widths of 50, 20, and 10 μm, while for the stripe width of 5 μm, the PL spectrum only has a single peak, similar to the PL spectrum from the intermixed sample. Thus, it is concluded that the spatial resolution is better than 5 μm. The interesting finding here is that in the sample annealed with a stress-inducing dielectric mask, the dual peaks of PL spectra are better defined for the stripe widths of 50, 20, and 10 μm, and are even discernible at the stripe width of 5 μm. From these observations, the spatial selectivity is determined to be less than 2.5 μm, which is half of the narrowest stripe width at the dual peak spectra from sample annealed with a stress-inducing dielectric mask.

Due to the limitation of the deduced spatial resolution from PL measurements, MRS measurement was used to reveal the information of the disordered alloy across the boundary between intermixed and unintermixed regions from the compositional change after the plasma-enhanced QWI process. A sample of InGaAs/InGaAsP QWs laser structure with a pattern of variable stripe widths (with Si_xN_y patterns that are hundreds of micrometers wide) was exposed and annealed with the presence of stress-inducing dielectric masks. After the QWI process and dielectric mask removal, the selective chemical etchants (H_2SO_4 : H_2O_2 : H_2O solution and subsequent HCl : H_3PO_4 solution) were used to remove the InGaAs/InGaAsP contact layers and the InP upper cladding, respectively. The wet etching removal was controlled carefully with the routine check procedure using an unprocessed QW sample measured using a surface profiler. The removal of the contact layers and upper cladding layers will provide the direct information of compositional changes close to the QW active region across the boundary, in contrast to the experiment done by Ong *et al.*, where the spatial resolution was measured from the contact layers [26].

PL measurement at 77 K using an optical fiber probe were performed at the intermixing boundary to check the compositional intermixing of QWs after the subsequent top section removal. From Fig. 6(a), a well-separated dual peak spectrum corresponding to the sum of intermixed and unintermixed signals is observed, indicating the presence of the QW active region after the wet etch process and supporting the previous experiment using variable stripe widths of patterned area that the spatial resolution of the process is better than the optical fiber diameter of 50 μm. The PL peak at 1441 nm is attributed to the unintermixed region while the PL peak at 1366 nm is from the intermixed region. The PL measurement from the as-grown sample showed a PL peak of 1456 nm, indicating that the annealing process caused the thermal shift of 15 nm on

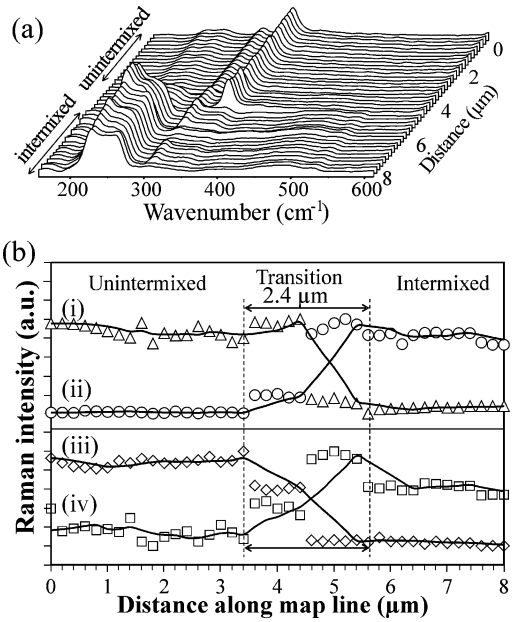

Fig. 7. (a) Three-dimensional view of the line map Raman spectra taken from the intermixed (denoted as 0 μm) to the unintermixed region indicates the spatial resolution from the Raman spectra transition. (b) The Raman amplitude-mode varies across the 8 μm-scan line: (i) I_{InAs}; (ii) I_{GaP}; (iii) I_{GaAs}/I_{InAs}; and (iv) I_{GaP}/I_{InP}. The solid lines are to guide the eyes, using an average of five data points.

the masked region. The dual peak PL spectrum shows a nearly perfect line shape fit with two Gaussian curves. The absence of any appreciable linewidth difference between two regions from the Gaussian fits suggests that the plasma-enhanced QWI does not introduce any significant degradation of optical quality with respect to the protected region during plasma exposure. In addition, the RT PL mapping was measured to provide the uniformity of bandgap distribution profile from sample annealed with a stress-inducing dielectric mask. The resolution of the PL mapping system is 100 μm, which is the smallest step size of mapping scan. Fig. 6(b) shows the two-dimensional map profile and one-dimensional line profile of PL peak distribution across the selectively intermixed sample revealing the distinct dual bandgap across the sample with a good uniformity across the selectively intermixed sample with dimension of 1.2×1.2 mm. It is worth noting that the uniform PL linewidth distribution (not shown here) provides a further evidence of the optical quality preservation of the intermixed QWs.

Helmy *et al.* found that the MRS was suitable as a sensitive technique for characterizing QWI processes with high spatial resolution by studying features of the Raman-mode spectra, such as relative mode amplitudes and integrated mode area [27]. Such variation in the amplitude-peak mode due to the interdiffusion of atoms in InGaAsP alloys is related to the relative density of corresponding bonds [28]–[31]. The change in Raman peak intensity and its ratio between the two consecutive Raman spectra across the intermixing boundary indicates the spatial resolution of the QWI process due to compositional alterations that modifies the vibrational properties of the crystal lattice. A uniform penetration depth of $\sim$90 and $\sim$110 nm below the sample surface is predicted from the calculation of its absorption length directly for InP and GaAs material, respectively [32]. Thus, the Raman modes with the largest signal-to-noise ratio were dominantly generated from the InGaAsP GRIN layers of the QW active region. Fig. 7(a) shows a unique variation of Raman spectra in the transition region between the intermixed and unintermixed area taken from 3.6 to 6 μm spatial distances, unambiguously indicating the interdiffusion process has started beneath the masked region due to the atomic lateral diffusion of the QWI process. The resulting line map Raman spectra were further analyzed, by monitoring the amplitude-mode of InAs (I_{InAs})- and GaP (I_{GaP})-like LO phonon peaks together with the amplitude-mode ratio (I_{InAs}/I_{GaAs} and I_{GaP}/I_{InP}) to reveal the extent of lateral diffusion across intermixing boundary [30], [31], as depicted in Fig. 7(b). The similar lateral transition trends were obtained for GaAs (I_{GaAs})- and InP (I_{InP})-like LO phonon peaks with lower amplitude-mode contrasts, which are not shown here. An obvious decrease in the GaP-like LO mode amplitude with an increase in the InAs-like LO mode amplitude at a separation of 2.4 μm was observed that is similar to the amplitude-mode ratio transition across the map line. These transitions unambiguously indicate that the spatial resolution from the laterally compositional interdiffusion is about 2.4 μm. This value from MRS study was consistent to the spatial resolution obtained using PL measurements, indicating that the stress-inducing dielectric mask improves the spatial resolution of Ar plasma-induced QWI to $\sim$ 2.4 μm.

The intermixing of QWs under the masked region could be due to the combined effects of: 1) lateral spread of surface defects during Ar plasma exposure and 2) lateral diffusion of defects during annealing. The improvement of spatial resolution is ascribed to the existence of the stress-inducing dielectric mask, which provided the vertical stress across the mask interface during annealing [33]. The edges of the dielectric mask cause the modulation of the material stress during the annealing stage due to the large difference in the thermal coefficient expansion between the Si_xN_y layer and the QW material. The compressive state of the QW material under the Si_xN_y masked region generates a higher compressive strain at the pattern edge and thus forming the stress field lines oriented in a direction perpendicular to the sample surface. The vertical stress field lines act as a barrier to limit the point defect diffusion in the lateral direction, since it is difficult for the mobile point defects to move across the vertical stress field lines due to the presence of the stress-inducing dielectric mask. As a result, the vertical stress will minimize the lateral diffusion of point defects underneath the mask during annealing, thus giving rise to an improvement of spatial resolution, i.e., $\sim$ 2.4 μm analyzed from the PL and the MRS measurements.

V. One-Step Multiple Bandgap Creation

The lateral control of bandgap across a single chip is crucial for the implementation of PICs because different optical components on a PIC module commonly have different bandgap requirements. Since most defects are introduced on the near sample surface during plasma exposure, the lateral diffusion of defects below the spatial resolution of plasma-induced QWI can be utilized to modulate the defect concentration reaching the QW active region using a spatially masked pattern; thus, different degrees of the intermixing can be obtained in single expo-

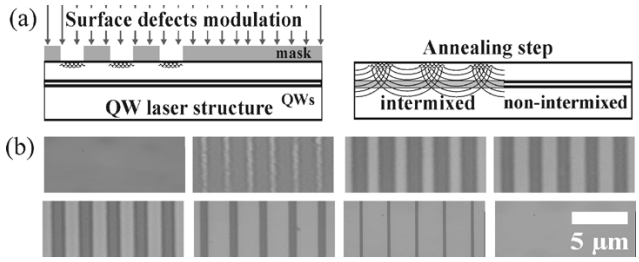

Fig. 8. Schematic representation of the spatial control of intermixing degree. (a) The surface defects modulation during plasma exposure using a 300-nm-thick SiO_2 mask layer. (b) The annealing step to induce different degree of intermixing. The high mobility of mobile point defects on the near sample surface leads to the uniform distribution at the QW active region for modulated area of smaller than the lateral diffusion length. (c) The optical microscope picture of the 8 different exposed area coverage (dark area) using 2.5-μm stripe SiO_2 layer (bright area) as a defects modulation mask, varying from 0% [top left], 30%, 40%, 45%, 50%, 75%, 90%, and 100% (bottom right).

sure-annealing step. The spatial defect modulated intermixing (SDMI) takes advantage of the lateral defect migration during annealing similar to the multiple-bandgap approach in the IFVD technique [4], by varying the window exposure area percentage, below its spatial resolution investigated in the previous section, as depicted in Fig. 8(a).

Two samples of InGaAs/InGaAsP QWs laser structure were deposited with a 300-nm-thick SiO_2 layer by electron beam evaporation and spin-coated with a 1.5-μm-thick AZ 5214 photoresist. The photoresist layer was patterned into eight stripe arrays and transferred to the SiO_2 layer in a CF_4/O_2 RIE process followed by photoresist removal, so that, as shown in Fig. 8(b), the areas opened to plasma exposure in the stripe arrays were 0%, 30%, 40%, 45%, 50%, 75%, 90%, and 100% of the 2.5-μm-wide stripe array areas as a control mask, respectively. The pattern samples were exposed to Ar plasma for 5 min. After the SiO_2 removal using diluted HF solution, a subsequent annealing was done at 600 °C for 2 min. The SiO_2 removal prior to annealing is necessary to improve the lateral defect migration for the given stripe widths, as suggested from the previous spatial resolution study without the stress-inducing dielectric mask. PL spectra at 77 K were measured using a similar optical fiber probe to each array.

Fig. 9 summarizes the measured PL spectra and the corresponding bandgap shifts and linewidths of InGaAs/InGaAsP QW laser structure. Only a small variation of the linewidth was observed as the exposure coverage increases and the PL spectra did not appear to be double peaked, suggesting that the intermixing process is uniform with 2.5-μm-wide diffusion control mask. The 0% exposed area was found to be almost fully inhibited from intermixing, while 100% exposed area was intermixed by about 100 nm (66 meV). The degree of intermixing increases linearly as the exposed percentage area increases indicating that the correlation between the amount of created mobile defects on the surface and the achieved degree of bandgap shift, similar to that in the case of QWI using IID using ion implantation [18]. The linear dependency underscores that the single-step multiple bandgap process permits the implementation of multiple wavelength control across a substrate with a simple and reliable semiconductor processing technology. This spatial defect modulation approach can be widely applied to achieve multiple bandgap with other existing QWI techniques.

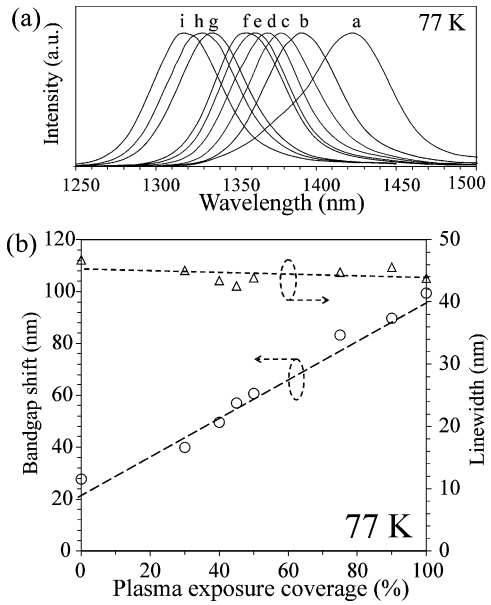

Fig. 9. (a) 77 K PL spectra of intermixed InGaAs/InGaAsP QWs laser structure different window exposure areas (a—as-grown, b—0%, c—30%, d—40%, e—45%, f—50%, g—75%, h—90%, and i—100%) of the 2.5-μm-wide stripe control mask. (b) The correlation between bandgap shift and the linewidth as compared to the as-grown material versus percentage of window exposure area.

VI. Photonic Integrated Device: Extended Cavity Laser

The monolithic integration of an active laser and a low-loss passive waveguide in the form of an extended cavity laser (ECL), which is transparent to the laser emission, is an essential step toward the realization of PIC technology [34]. Such integration is thus of great importance for monolithically integrated tunable laser diodes, low-loss distributed Bragg reflector lasers, lasers integrated with optical modulators, high-power grating-coupled emission lasers, superluminescent diodes, and integrated extended cavity mode-locked lasers. Since the Ar plasma-induced QWI is an impurity free process, the demonstration of low loss waveguide is extremely demanded. Losses introduced by nonradiative recombination centers of by free carriers, as in IID technique, are expected to be significantly reduced.

From Fig. 10(a), the bandgap at passive waveguide sections were selectively intermixed in order to reduce the propagation loss at the lasing wavelength from the unintermixed active laser section. A sample of InGaAs/InGaAsP QWs laser structure with a pattern of variable stripe widths (with hundreds-of-micrometers-wide SiO_2 patterns as an intermixing mask) was exposed under Ar plasma for 5 min and annealed. Fig. 10(b) shows the normalized PL spectra at 77 K obtained from the partially masked sample. The masked section has 6-nm bandgap shift and 5.2-nm linewidth broadening, which is attributed to thermal shift. The unmasked section has a much larger bandgap shift of 92 nm, thus producing a bandgap difference of 86 nm with a small differential linewidth broadening of 0.3 nm. These results imply the high selectivity obtainable using 200-nm-thick SiO_2 layer as intermixing mask with good preservation of optical quality from the minimal linewidth broadening. Following the intermixing step, the broad area ECLs was fabricated. The removal of the 150-nm-thick highly doped InGaAs/InGaAsP

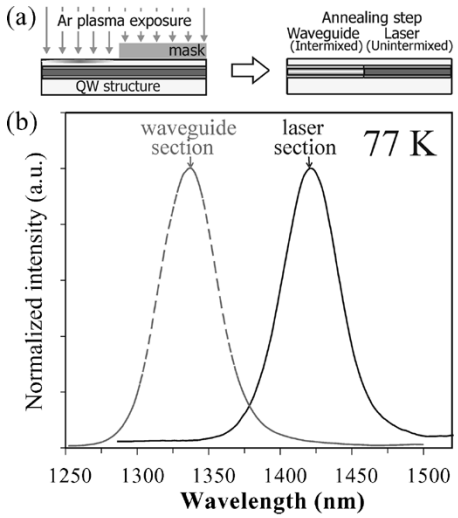

Fig. 10. (a) A schematic diagram showing the low loss waveguide fabrication integrated with a laser device in the form of extended cavity laser. (b) The 77 K PL spectra from the selectively intermixed InGaAs/InGaAsP QWs laser structure partially masked with a 200-nm-thick SiO_2 layer during Ar plasma exposure. The differential bandgap shift was 86 nm between masked (solid line) and unmasked section (dashed line).

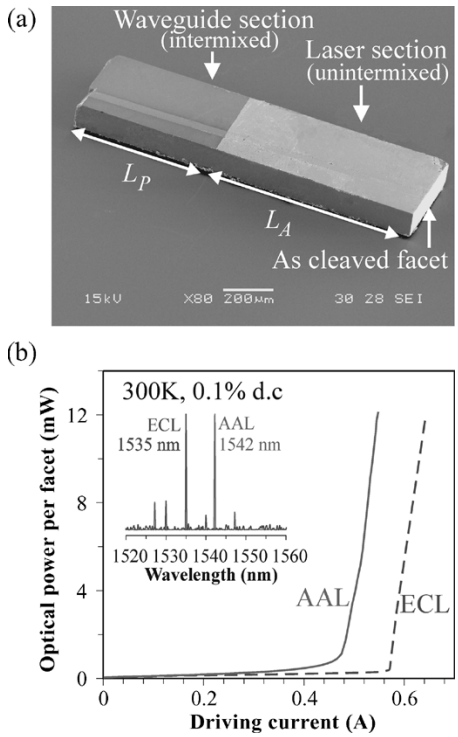

Fig. 11. (a) Scanning electron microscopy (SEM) picture of fabricated broad area ECL with 50-μm-wide active window for current injection. All individual ECL was 400 μm wide, the length of active section was 800 μm, and the passive section lengths of lasers were varied. (b) The L-I characteristics of an broad area ECL (dotted line) with active (passive) length of 800 μm (1200 μm) and AAL (solid line) with 800-μm cavity length The measurement was done at RT with pulse driving current with 0.1% duty cycle.

cap layer minimizes current spreading into the passive section and the absorption of light in this section. A 200-nm-thick SiO_2 was deposited using PECVD and a 50-μm contact window was defined using dry etch in RIE machine followed by wet etch. A p-contact of Ti/Au layers was defined over the laser active sections using a liftoff process to ensure electrical isolation between active and passive sections. The sample was then thinned down and n-metal contact of Au/Ge/Au/Ni/Au layers was formed and alloyed using rapid thermal processor. The final ECLs devices [as shown in Fig. 11(a)] were tested at RT under pulsed current operation (1% duty cycle). Fig. 11(b) shows the plot of light output versus injected current (L-I) characteristics of 800-μm-long active section lasers with passive section length of 1200 μm. For comparison, 800-μm-long all active lasers (AAL) were cleaved from the same sample. The threshold current was increased by 18% from 481 mA for AAL to 569 mA, which can be attributed to diffractive losses within intermixed passive section. The slope efficiency undergoes a little decrease by 9%, from 0.174 W/A to 0.159 W/A per facet. As shown in the inset of Fig. 11(b), the wavelength emission of ECL exhibits an apparent blue-shift (1.535 μm) as compared to unprocessed AAL laser (1.542 μm). The 7-nm blue-shift in wavelength emission might be due to the band filling effect from the increase in threshold current in the ECL rather than the graded bandgap on the passive–active interface due to the plasma-induced QWI process, as revealed from the spatial resolution study earlier. This shift of the wavelength will cause the propagation losses to increase slightly, since the energy of the photons is now closer to the bandgap of the passive waveguide section.

From the L-I characteristics, it is possible to define the relationship between AAL threshold current (I_{AA}), ECL threshold current (I_{ECL}), and the propagation loss in the passive section (α_P). The threshold currents are related by the formula [35]

$$\ln\left(\frac{I_{\mathrm{ECL}}}{I_{\mathrm{AA}}}\right) = \frac{\alpha_P L_P + \ln\left(\frac{1}{\kappa}\right)}{\Gamma g_0 L_A} \tag{1}$$

where L_A and L_P are lengths of the active and passive sections; g_0 is the gain of the active structure; κ is the optical transmission coefficient at the interface of the active to passive sections; and Γ is the overlap integral within the QWs. An estimated value of $\Gamma g_0 \sim 30\ \mathrm{cm}^{-1}$ was used [36] and κ is obtained from the QWI-induced refractive index change with a calculated step profile to be 0.999 998. This value of κ confirms that negligible reflection occurs at the passive/active interface. Comparing ECL with active (passive) length of 800 μm (1200 μm) and AAL with 800 μm cavity length, α_P is calculated to be 2.98 cm^{-1} or 12.9 dBcm^{-1}, which corresponds to about 2.6 dBcm^{-1} per well. The increase of threshold current density partly is ascribed to the divergence of the lasing mode within the extended cavity, which reduces the amount of light returning to the pumped laser region. Taking into account the interface reflectivity due to the spatially graded interdiffusion profile and lateral optical spreading loss of 7.9% at the active-passive interface, the corrected value of waveguide loss α_P is 2.3 cm^{-1}. If compared to the LID technique, the estimated residual loss here was comparable to the calculated loss (2.4 cm^{-1}) from the ECL with a similar active length of 800 μm and slightly higher than to the pure ridge waveguide loss of 2.1 cm^{-1} measured using Fabry–Pérot measurement [36]. The quantum efficiency degradation in the presence of integrated passive section can be expressed as [37]

$$\frac{\eta_{\mathrm{ECL}}}{\eta_{\mathrm{AA}}} = \frac{\alpha_A + \frac{1}{L_A}\ln\frac{1}{R}}{\alpha_A + \frac{1}{L_A}\ln\frac{1}{R} + \alpha P\frac{L_P}{L_A}} \tag{2}$$

where R is the facet reflectivity, calculated to be 0.27 for the as-cleaved structure. The ratio calculated with the above equation is 0.87, which is in agreement with the measured value of 0.91 from the L-I characteristics. This small discrepancy can be explained by noting that the effective length of gain section is shorter than the physical active pumped section due to the graded bandgap interface region after intermixing, which can lead to increase in the threshold current without any contribution to the gain.

VII. Conclusion

The capability of plasma-induced QWI technique for high-density photonic integrated devices has been investigated on three aspects: 1) universality to the wide range of III–V materials; 2) spatial resolution; and 3) single-step multiple bandgap creation. High plasma density due to ICP application has been found to contribute in promoting the intermixing in QW structures besides the pure ion bombardments while preserving the optical quality after the process. The analysis from the intermixing process of GaAs/AlGaAs multiwidth QWs damage probe structure reveals that the point defects are created at near sample's surface during plasma exposure and upon the subsequent annealing, they propagate deeper to a depth beyond ~ 2.32 μm to promote intermixing between well and barrier. The demonstration of tuning the GaAs/AlGaAs and InGaAs/InAlGaAs QWs in addition to the InGaAs/InGaAsP QWs underscores the universal QWI process in a wide range of the GaAs-based and InP-based material.

We have investigated the effect of the dielectric mask induced stress to the spatial resolution of plasma-enhanced QWI. The presence of dielectric mask induced stress gives an improvement in the spatial resolution to ~ 2.4 μm, which might be applicable for the spatial resolution improvement in various shallow defect-induced QWI techniques, such as using low energy ion implantation, sputtered silica deposition, anodic-oxide-induced interdiffusion, low-temperature InP, and excimer laser-induced disordering, in a simple way. Utilizing the lateral diffusion of defects below the spatial resolution of plasma-induced QWI, a simple and reliable way to obtain a controlled multiple bandgap was achieved by using the spatial defect modulated intermixing using control dielectric mask with variable window exposure area. Eight bandgap levels were realized using single exposure-annealing step with a linear relationship to the fraction of the open area under plasma exposure. Eventually, the simple photonic integration has been demonstrated using the plasma-induced QWI process in the form of extended cavity lasers. A low-loss extended cavity laser has been fabricated with the measured waveguide loss as low as 2.1 cm^{-1} with 1200-μm-long passive waveguide.

These results highlight the capability of plasma-induced QWI technique in the application of high-density photonic integration, allowing the realization of multiple-section photonic device across a single chip using a one-step processing technique. This work provides an alternative approach of QWI by adopting conventional process available in the semiconductor industry and thus may bring the impact to the development of PICs technology.

Note: During the paper communication, the plasma-induced QWI technique has also been adopted to reduce the absorption loss in asymmetric twin waveguide laser tapers [38] and to realize the wavelength monitoring with low-contrast multimode interference waveguide [39].

References

[1] J. H. Marsh, O. P. Kowalski, S. D. McDougall, B. C. Qiu, A. McKee, C. J. Hamilton, R. M. De La Rue, and A. C. Bryce, "Quantum well intermixing in material systems for 1.5 μm," *J. Vac. Sci. Technol. A*, vol. 16, pp. 810–816, 1998.

[2] S. Charbonneau, E. S. Koteles, P. J. Poole, J. J. He, G. C. Aers, H. Haysom, M. Buchanan, Y. Feng, A. Delage, F. Yang, M. Davies, R. D. Goldberg, P. G. Piva, and I. V. Mitchell, "Photonic integrated circuits fabricated using ion implantation," *IEEE J. Sel. Topics Quantum Electron.*, vol. 4, no. 4, pp. 772–793, Jul./Aug. 1998.

[3] V. Aimez, J. Beauvais, J. Beerens, D. Morris, H. S. Lim, and B. S. Ooi, "Low-energy ion-implantation-induced quantum-well intermixing," *IEEE J. Sel. Topics Quantum Electron.*, vol. 8, no. 4, pp. 870–879, Jul./Aug. 2002.

[4] B. S. Ooi, K. McIlvaney, M. W. Street, A. S. Helmy, S. G. Ayling, A. C. Bryce, J. H. Marsh, and J. S. Roberts, "Selective quantum-well intermixing in GaAs–AlGaAs structures using impurity-free vacancy diffusion," *IEEE J. Quantum Electron.*, vol. 33, no. 10, pp. 1784–1793, Oct. 1997.

[5] S. P. McDougall, O. P. Kowalski, C. J. Hamilton, F. Camacho, B. Qiu, M. Kee, R. M. De La Rue, A. C. Bryce, and J. H. Marsh, "Monolithic integration via a universal damage enhanced quantum well intermixing technique," *IEEE J. Sel. Topics Quantum Electron.*, vol. 4, no. 4, pp. 636–646, Jul./Aug. 1998.

[6] B. S. Ooi, T. K. Ong, and O. Gunawan, "Multiple-wavelength integration in InGaAs–InGaAsP structures using pulsed laser irradiation induced quantum well intermixing," *IEEE J. Quantum Electron.*, vol. 40, no. 5, pp. 481–490, May 2004.

[7] E. J. Skogen, J. S. Barton, S. P. Denbaars, and L. A. Coldren, "A quantum-well-intermixing process for wavelength-agile photonic integrated circuits," *IEEE J. Sel. Topics Quantum Electron.*, vol. 8, no. 4, pp. 863–869, Jul./Aug. 2002.

[8] H. S. Djie, J. Arokiaraj, T. Mei, X. H. Tang, L. K. Ang, and D. Leong, "Large blue-shift in InGaAs/InGaAsP laser structure using inductively coupled Argon plasma enhanced quantum well intermixing," *J. Vac. Sci. Technol. B*, vol. 21, pp. L1–L4, Jul./Aug. 2003.

[9] H. S. Djie, T. Mei, J. Arokiaraj, and P. Thilakan, "High-density plasma enhanced quantum well intermixing in InGaAs/InGaAsP structure using Argon plasma," *Jpn. J. Appl. Phys.*, vol. 41, pp. L867–L868, 2002.

[10] H. S. Djie, C. Sookdhis, T. Mei, and J. Arokiaraj, "Photonic integration using inductively coupled Argon plasma enhanced quantum well intermixing," *Electron. Lett.*, vol. 38, pp. 1672–1673, 2002.

[11] B. S. Ooi, A. C. Bryce, and J. H. Marsh, "Integration process for photonic integrated circuits using plasma damage induced layer intermixing," *Electron. Lett.*, vol. 31, pp. 449–451, 1995.

[12] M. Schultz, U. Egger, R. Scholz, O. Breitenstein, U. Gosele, and T. Y. Tan, "Experimental and computer simulation studies of diffusion mechanisms on the arsenic sublattice of gallium arsenide," *J. Appl. Phys.*, vol. 83, pp. 5295–5301, 1998.

[13] H. F. Wong, D. L. Green, T. Y. Liu, D. G. Lishan, M. Bellis, E. L. Hu, P. M. Petroff, P. O. Holtz, and J. L. Merz, "Investigation of reactive ion etching induced damage in GaAs-AlGaAs quantum well structures," *J. Vac. Sci. Technol. B.*, vol. 6, pp. 1906–1910, 1988.

[14] B. S. Ooi, A. C. Bryce, C. D. W. Wilkinson, and J. H. Marsh, "Study of reactive ion etching-induced damage in GaAs/AlGaAs structures using a quantum well intermixing probe," *Appl. Phys. Lett.*, vol. 64, pp. 598–600, 1994.

[15] H. S. Djie, T. Mei, J. Arokiaraj, C. Sookdhis, S. F. Yu, L. K. Ang, and X. H. Tang, "Experimental and theoretical analysis of Argon plasma enhanced quantum well intermixing," *IEEE J. Quantum Electron.*, vol. 40, no. 2, pp. 166–174, Feb. 2004.

[16] M. Rahman, L. G. Deng, J. Van Den Berg, and C. D. W. Wilkinson, "Minimization of dry etch damage in III–V semiconductors," *J. Phys. D, Appl. Phys.*, vol. 34, pp. 2792–2797, 2001.

[17] D. Lootens, P. Van Daele, P. Demeester, and P. Clauws, "Study of electrical damage in GaAs induced by $SiCl_4$ reactive ion etching," *J. Appl. Phys.*, vol. 70, pp. 221–224, 1991.

[18] P. J. Poole, S. Charbonneau, G. C. Aers, T. E. Jackman, M. Buchanan, M. Dion, R. D. Goldberg, and I. V. Mitchell, "Defect diffusion in ion implanted AlGaAs and InP: consequences for quantum well intermixing," *J. Appl. Phys.*, vol. 78, pp. 2367–2371, 1995.

[19] D. L. Green, E. L. Hu, and N. G. Stoffel, "Effect of superlattices on the low-energy ion-induced damage in GaAs/Al(Ga)As structures: channeling or diffusion?," *J. Vac. Sci. Technol. B*, vol. 12, pp. 3311–3316, 1994.

[20] S. Janz, M. Buchanan, P. van der Meer, Z. R. Wazilewski, D.-X. Xu, P. Piva, I. V. Mitchell, U. G. Akano, and A. Fiore, "Patterning the second-order optical nonlinearity of asymmetric quantum wells by ion implantation enhanced intermixing," *Appl. Phys. Lett.*, vol. 72, pp. 3097–3099, 1998.

[21] A. S. Helmy, D. C. Hutchings, T. C. Kleckner, J. H. Marsh, A. C. Bryce, J. M. Arnold, C. R. Stanley, J. S. Aitchison, C. T. A. Brown, K. Moutzouris, and M. Ebrahimzadeh, "Quasi phase matching in GaAs-AlAs superlattice waveguides through bandgap tuning by use of quantum-well intermixing," *Opt. Lett.*, vol. 25, pp. 1370–1372, 2000.

[22] M. Kuzuhara, T. Nozaki, and T. Kamejima, "Characterization of Ga out-diffusion from GaAs into SiO_xN_y films during thermal annealing," *J. Appl. Phys.*, vol. 66, pp. 5833–5836, 1989.

[23] A. Pepin, C. Vieu, M. Schneider, H. Launois, and Y. Nissim, "Evidence of stress dependence in SiO_2/Si_3N_4 encapsulation-based layer disordering of GaAs/AlGaAs quantum well heterostructures," *J. Vac. Sci. Technol. B*, vol. 15, pp. 142–153, 1997.

[24] K. S. Chan, Y. H. Wong, E. Y. B. Pun, H. P. Ho, and P. S. Chung, "A theoretical analysis of quantum-wire fabrication by vacancy-enhanced interdiffusion of quantum wells," *IEEE J. Sel. Topics Quantum Electron.*, vol. 4, no. 4, pp. 701–705, Jul./Aug. 1998.

[25] S. K. Si, D. H. Yeo, K. H. Yoon, and S. J. Kim, "Area selectivity of InGaAsP-InP multiquantum-well intermixing by impurity-free vacancy diffusion," *IEEE J. Sel. Topics Quantum Electron.*, vol. 4, no. 4, pp. 619–623, Jul./Aug. 1998.

[26] T. K. Ong, O. Gunawan, B. S. Ooi, Y. L. Lam, Y. C. Chan, Y. Zhou, A. S. Helmy, and J. H. Marsh, "High-spatial-resolution quantum-well intermixing process in GaInAs/GaInAsP laser structure using pulsed-photoabsorption-induced disordering," *J. Appl. Phys.*, vol. 87, pp. 2275–2279, 2000.

[27] A. S. Helmy, A. C. Bryce, C. N. Ironside, J. S. Aitchison, and J. H. Marsh, "Raman spectroscopy for characterizing compositional intermixing in GaAs/AlGaAs heterostructures," *Appl. Phys. Lett.*, vol. 74, pp. 3978–3980, 1999.

[28] T. Inoshita, "Long-wavelength lattice dynamics of $In_{1-x}Ga_xAs_yP_{1-y}$ alloys," *J. Appl. Phys.*, vol. 56, pp. 2056–2064, 1984.

[29] S. J. Yu, H. Asahi, S. Emura, and S. I. Gonda, "Raman scattering study of thermal interdiffusion in InGaAs/InP superlattice structures," *J. Appl. Phys.*, vol. 70, pp. 204–208, 1991.

[30] S. J. Yu, H. Asahi, J. Takizawa, S. Emura, S. Gonda, H. Kubo, C. Hamaguchi, and Y. Hirayama, "Disordering of InGaAs/InP superlattice and fabrication of quantum wires by focused Ga ion beam," *J. Vac. Sci. Technol. B*, vol. 9, pp. 2683–2686, 1991.

[31] T. Sugiura, N. Hase, Y. Iguchi, and N. Sawaki, "Raman intensity of phonon modes in InGaAsP quartenary alloys grown on (100) InP in the region of immiscibility," *Jpn. J. Appl. Phys.*, vol. 38, pp. 996–1000, 1999.

[32] D. E. Aspnes and A. A. Studna, "Dielectric functions and optical parameters of Si, Ge, GaP, GaAs, GaSb, InP, InAs, and InSb from 1.5 to 6.0 eV," *Phys. Rev. B*, vol. 27, pp. 985–1009, 1983.

[33] A. Pepin, C. Vieu, M. Schneider, R. Planel, J. Bloch, G. B. Assayag, H. Launois, J. Y. Marzin, and Y. Nissimb, "GaAs/AlGaAs quantum wires fabricated by SiO_2 capping-induced intermixing," *Appl. Phys. Lett.*, vol. 69, pp. 61–63, 1996.

[34] N. K. Dutta, T. Cella, A. B. Piccirilli, and R. L. Brown, "Integrated external cavity laser," *Appl. Phys. Lett.*, vol. 49, pp. 1227–1229, 1986.

[35] J. Werner, E. Kapon, N. G. Stoffel, E. Colas, S. A. Schwarz, C. L. Schwartz, and N. Andreadakis, "Integrated external cavity GaAs/AlGaAs lasers using selective quantum well disordering," *Appl. Phys. Lett.*, vol. 55, pp. 540–542, 1988.

[36] B. C. Qiu, A. C. Bryce, R. M. De La Rue, and J. H. Marsh, "Monolithic integration in InGaAs-InGaAsP multiquantum-well structure using laser processing," *IEEE Photon. Technol. Lett.*, vol. 10, no. 6, pp. 769–771, Jun. 1998.

[37] A. C. Bryce, F. Camacho, P. Cusumano, and J. H. Marsh, "CW and mode-locked integrated extended cavity lasers fabricated using impurity free vacancy disordering," *IEEE J. Sel. Topics Quantum Electron.*, vol. 3, no. 3, pp. 885–892, Jun. 1997.

[38] Y. Huang, F. Xia, V. M. Menon, S. R. Forrest, and M. Gokhale, "Reduction of absorption loss in asymmetric twin waveguide laser tapers using Argon plasma-enhanced quantum-well intermixing," *IEEE Photon. Technol. Lett.*, vol. 16, no. 10, pp. 2221–2223, Oct. 2004.

[39] C. Sookdhis, T. Mei, and H. S. Djie, "Wavelength monitoring with low-contrast multimode interference waveguide," *IEEE Photon. Technol. Lett.*, vol. 17, no. 4, pp. 822–824, Apr. 2005.

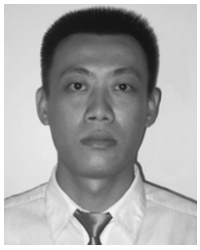

Hery Susanto Djie (S'03–M'04) received the B.Eng. degree (first-class honors) in electrical engineering from Pelita Harapan University in 1999, under a Lippo Group Scholarship, and the Ph.D. degree from the Photonics Research Centre, School of Electrical and Electronic Engineering, Nanyang Technological University, Singapore, in 2004.

He was an Epitaxy Engineer at Agilent Technologies, Singapore. He is currently a Postdoctoral Researcher with the Center for Optical Technologies, Department of Electrical and Computer Engineering, Lehigh University, Bethlehem, PA. During his Ph.D. study, he published over 50 international technical papers in the field of III–V quantum heterostructure intermixing. His current research interests are the physics of low-dimensional quantum heterostructures, the plasma-based semiconductor process, quantum heterostructure intermixing, single mode/tunable laser diode, the ultrabroadband superluminescent diode, high-brightness light emitting diodes and optoelectronics/photonics integrated circuits.

Dr. Djie has been a Student Member and Member of the IEEE Lasers and Electro-Optics Society (LEOS) since 2003 and 2004, respectively.

Ting Mei (M'00) received the B.S. and M.S. degrees in optical engineering from Zhejiang University in 1988 and 1991, respectively, and the Ph.D. degree in electrical engineering from the National University of Singapore in 2000.

He was a Research Staff Member for Zhejiang University, China, and the Institute of Microelectronics, Singapore, from 1991 to 1995 and 1997 to 2000, respectively. He is currently an Assistant Professor of Electrical and Electronic Engineering at Nanyang Technological University, Singapore. He has publications on quantum well intermixing, photonic integration, quantum well infrared photodetectors, and micromachined infrared bolometers. His research areas have included optoelectronics, compound semiconductor quantum devices, silicon microelectromechanical systems (MEMS) devices and infrared imaging technology. He is now investigating the integration of photonic active and passive devices.

Prof. Mei has been a Member of the IEEE Lasers and Electro-Optics Society (LEOS) since 2000.